Temporal estimation of corn (*Zea mays L.*) yield using GRAMI model, satellite imagery, and climate data in a semi-arid area

Fatemeh Asghari[1*], Mohammad Sharif[2], Mirmasoud Kheirkhah Zarkesh[3], Jahangir Porhemmat[3]

(1. Department of GIS/RS, Faculty of Natural Resources and Environment, Science and Research Branch, Islamic Azad University, Tehran, 14778-93855, Iran

2. Department of Geography, Faculty of Humanities, University of Hormozgan, Bandar Abbas, 3995, Iran

3. Soil Conservation and Watershed Management Research Institute, Agricultural Research Education and Extension Organization, Tehran, 13445-1136, Iran)

Abstract: Corn yield estimation constitutes a critical issue in agricultural management and food supply, especially in demographic pressure and climate change contexts. In light of precision and smart agriculture, this study aims to develop a diagnostic approach to temporally monitor and estimate corn yields using GRAMI (a model for simulating the growth and yield of grain crops), satellite images, and climate data at regional scale. The GRAMI-corn model is controlled by vegetation indices (VIs) derived from Landsat 8 satellite images and calibrated by climate data. The model was performed and validated using information collected from twenty five cornfields in a semiarid region in Ravansar, Iran. The average of under- or over-estimate yields was 919 k g h a $^{-1}$. In addition, the absolute error between the average observed and estimated yield values for the region was 19.21% for the 2016 corn season. The results using the GRAMI-corn model showed an acceptable agreement with field measurements.

Keywords: crop modeling, maize monitoring, product, remote sensing, Landsat 8, Ravansar

Citation: Asghari, F., M. Sharif, M. K. Zarkesh, and J. Porhemmat. 2022. Temporal estimation of corn (*Zea mays* L.) yield using GRAMI model, satellite imagery, and climate data in a semi-arid area. Agricultural Engineering International: CIGR Journal, 24(1): 26-40.

1 Introduction

Temporal monitoring of crop conditions and crop yields have been appeared as the main elements of sustainable agricultural management (Doraiswamy et al., 2003). Governmental, agricultural, and insurance agencies rely on acreage under crop cultivation to organize economic and social tasks including food supply and security, import and export markets, humanitarian aids, etc. from local to global scales. Among the agricultural products, corn (*Zea mays L.*) is an important staple food for human, forage for animal, and raw material for industrial products. Corn is the most cultivated cereals in the world. According to Food and Agriculture Organization (FAO), the world's harvested area of corn increased from 138 million ha in 1994 to 197 million ha in 2017. In addition, the production estimates increased from 568 million tons in 1994 to 1.134 billion tons in 2017

Received date: 2021-01-13 **Accepted date:** 2021-06-06

***Corresponding Author: Fatemeh Asghari,** M.Sc., Department of GIS/RS, Faculty of Natural Resources and Environment, Science and Research Branch, Islamic Azad University, Tehran, 14778-93855, Iran. Email: honey.asghari@gmail.com. Tel.: +982144865179.

(FAOSTAT, 2016). Based on FAO, the population of the world will have the growth of 35% by 2050 which reaches 9100 million residents, chiefly in developing countries. To prepare food for this population, food production needs to increase by 70%, in accordance with the safety and conservation of natural resources. Notably, some studies demonstrated that corn yield could diminish in the coming years due to anthropogenic climate change. Main impacts of climate change on agriculture are deterioration in crop yields, effects on production, consumption, and commercialization, and effects on per capita caloric consumption and child nutrition. Corn crop yield straightly rely on many contextual factors like management practices, the environment, genotype, and their interactions (Khaki et al., 2020; Sharif and Alesheikh, 2018). The influence of regional climate patterns and large-scale meteorological phenomena are able to have a remarkable impact on agricultural production (Dahikar and Rode, 2014). It is therefore necessary to have tools that enable real time corn yield monitoring and estimation over large areas.

One of the challenging problems in precision agriculture is crop yield prediction, and many models have been suggested and validated so far. This issue requires the use of a number of datasets since crop yield rely on many different factors such as climate, weather, soil, fertilizer usage, and seed variety (Xu et al., 2019). This illustrates that crop yield prediction is not a trivial task; instead, it involves several complicated steps. Presently, crop yield prediction models have the capability of estimating the real yield rationally, but a better performance in yield prediction is still favorable.

In light of smart agriculture and agronomy, remote sensing technology has been widely used in detection and classification of farmlands including corn yields (Atzberger and Eilers, 2011). A combination of visible, infrared, and microwave wavelengths of multi-band satellites, such as Landsat-8, Sentinel-1, and Sentinel-2, enables estimating and forecasting vigor, density, health, and productivity of crops (Drusch et al., 2012; Roy et al., 2014; Torres et al., 2012). By analyzing the spectral features of vegetation derived from satellite images, crop canopies, crop conditions, and crop yields can be easily observed over large areas. Crop modeling and remote sensing (RS) are both prevalent methodologies that suggest all the advantages of the techniques accessible for practical assessments of crop productivity and growth conditions (Nguyen et al., 2019). A crop model permits for sequential simulation, whereas RS enables consistency in the monitoring of geographic and spatial variations in crop conditions and productivity (Kim et al., 2015; Jeong et al., 2018b). The success of the remote sensing in crop modeling mainly originates in defining vegetation indices (VIs) as the primary explanatory indicator. However, crop modeling is still sensitive to soil and meteorological variables (e.g., temperature, precipitation, and moisture), which cannot be necessarily sensed on time, and need to be obtained from other sources (Moulin et al., 1998; Moran et al., 1995).

Several crop models have been proposed for the estimation of crop yields using satellite imagery (see reviews (Di Paola et al., 2016; Rauff and Bello, 2015; Oteng-Darko et al., 2013; Hoefsloot et al., 2012)). However, the functionality of a large number of them is dependent on the accuracy and completeness of input surface parameters (Ko et al., 2005). These initial parameters cannot be easily obtained at the corresponding regional areas (Padilla et al., 2012), which may consequently affect the crop models' performances. To overcome with the input parameterization constraint, various crop models have been introduced (e.g., GRAMI (Maas, 1992)) that not only employ fewer input parameters but also are faster to estimate crop production parameters (Ameline et al., 2018). The Gramineae (GRAMI)-crop model (Maas, 1993a, 1993b) was developed by the CESBIO laboratory to simulate the growth and yield of grain crops. GRAMI can use remotely sensed information (e.g., VI and land cover) for adjusting model parameters and reducing the gap between remote sensing estimate and model measurement of crop growth (Alharbi et al., 2019).

GRAMI has been validated for various crop types such as wheat (*Triticum spp.*), corn (*Zea mays L.*), sorghum (*Sorghum bicolor*), cotton (*Gossypium spp.*), and rice (*Oryza sativa*) in contrasting climatic conditions (Kim et al., 2017; Ko et al., 2005; Kim et al., 2015; Tashayo et al., 2020). The present form of GRAMI has been retitled as a RS-integrated crop model (RSCM), representing that the model is updated with the abovementioned information for future simulations of several crops variously. The RSCM allows the monitoring of croplands at different scales, ranging from farm fields to various geographical regions (Jeong et al., 2018a; Jeong et al., 2018b; Jeong et al., 2020; Yeom et al., 2018; Shawon et al., 2020).

Along with crop models, the contribution of climate data has been widely proved in the literature to estimate and measure crop production (Kamir et al., 2020; Basso and Liu, 2019). The influence of meteorological conditions on crop growth varies spatially and temporally (Butler and Huybers, 2013; Zipper et al., 2016). Meanwhile, the majority of the global models ignore the inherent correlation between the meteorological conditions in regions of study and crop yields (Van Ittersum et al., 2013; Van Wart et al., 2013). In this context, the objective of this study is to examine the GRAMI-corn model that is integrated with climate ancillary data for temporally monitoring grain corn yield derived from high spatial resolution satellite images.

2 Materials and methods

2.1 Site description

The city of Ravansar (34.34º N 46.39º E), which is located in the northwest of Kermanshah province, Iran, is selected as the area of interest (Figure 1). Ravansar's area is 1140 km^2 and lies 1343 m above sea level. Ravansar classified as Mediterranean climate meaning that it is sweltering and arid in summer, and very cold in winter. The temperature varies by 25.6°C from the warmest month (July) to the coldest month (January) with an average high-temperature of 6.5°C (43.7°F) and an average low-temperature of -4.3°C (24.3°F) of the year 2016 (May to September). The average annual temperature is 13.8°C (Climate-data, 2016). The climatic classification of Kermanshah province has been shown in Figure 2. Ravansar is characterized by sufficient annual precipitation (averages 551 mm) and susceptible agricultural lands for production of various crop species, such as wheat, barley, chickpea, and flint corn. This research selected 25 farms dedicated to corn production. The total area of the corn farms is 189 ha.

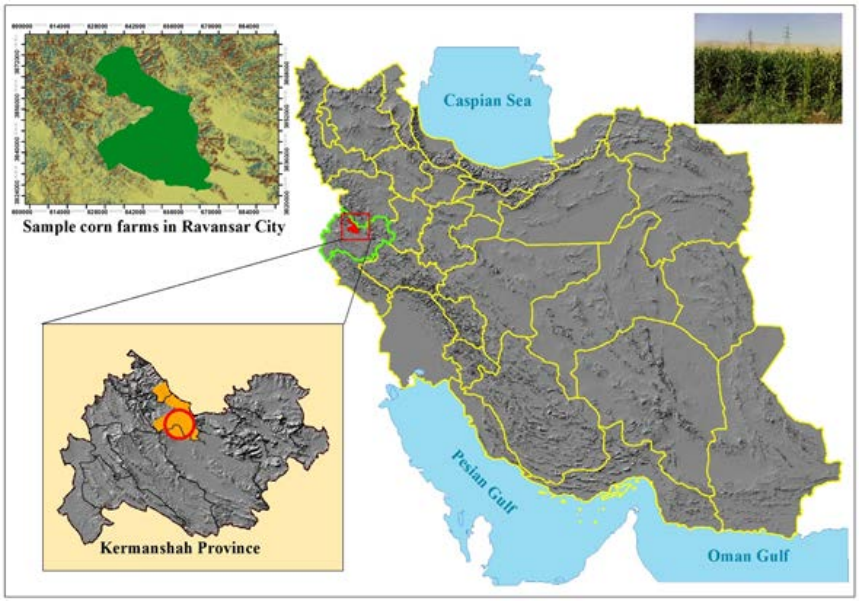

Figure 1 The study site: Ravansar, Kermanshah Province, Iran

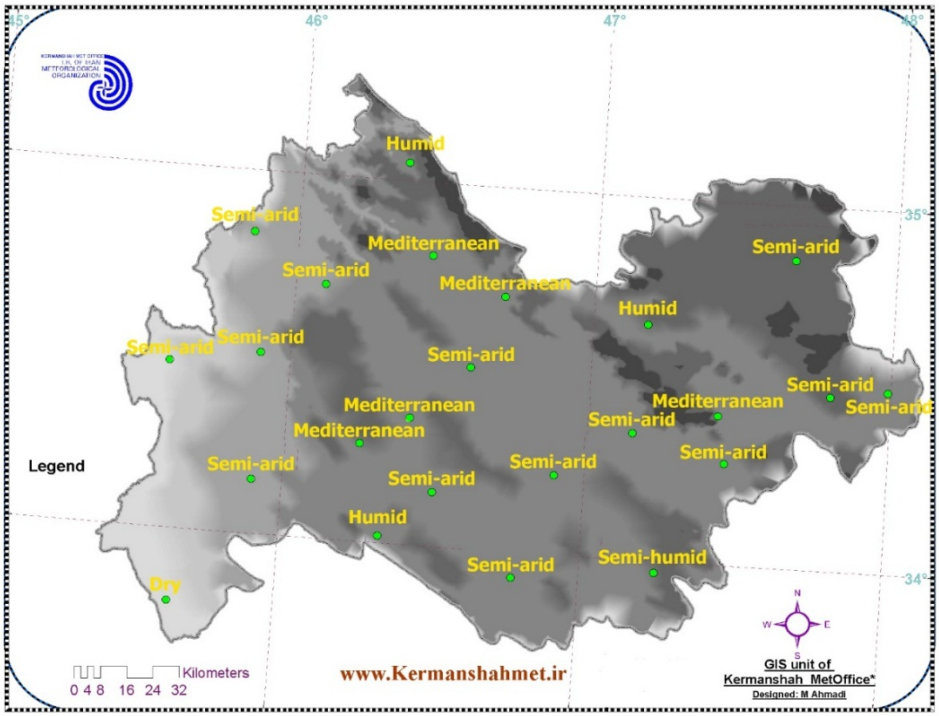

Figure 2 Climatic classification of Kermanshah Province

2.2 Data and pre-processing

In the current study, three data types namely satellite images, ground data, and climate records were employed. Pre-processing was performed on the dataset as follows.

Satellite Data: Five series of Landsat-8 images were acquired throughout corn cultivation period, from May to September 2016 (USGS, 2016). In terms of pre-processing, geometric correction was already applied on the images, and only the radiometric correction was performed. It should be noted that, this correction involves two steps called sensor and atmospheric correction in order to convert the digital number (DN) values of the data to spectral radiance and then to reflectance (both at the sensor). This is followed by the removal of atmospheric effects, which are due to absorption and scattering, to perform atmospheric correction (reflectance at the surface).

Ground Data: According to corn crop calendar in Ravansar, several queries and ground measurements were performed for each field to determine canopy growths and features including leaves dimensions, bushes heights, sampling points coordinates, phenological stages of the samples, fresh and wet weights of samples, irrigation period, and temperature at satellite crossing time. In addition, the AccuPAR LP-80 Ceptometer (Meter Group, USA) equipped with photosynthetically active radiation (PAR) sensor, was used for ground leaf area index (LAI) calculation. The obtained LAI map is compared with the normalized difference vegetation index (NDVI) map in Section 3.1. Throughout the crop season, the ground data were collected over 25 fields, in which 20 fields were used in calculations and five fields were used for validation and accuracy assessment.

Climate Data: Meteorological data including minimum and maximum daily air temperature were obtained from Kermanshah meteorological station (which is located 56 km far away from corn farms of the study) during the whole study season and the mean daily temperature was calculated. In addition, the average of monthly solar radiations was collected.

2.3 Methodology

A schematic overview of crop yield estimation using the GRAMI-corn model is illustrated in Figure 3. This procedure follows three steps of calculating NDVI and LAI from remote sensing data and ground data, respectively, and developing the GRAMI model by using

climate data and LAI map.

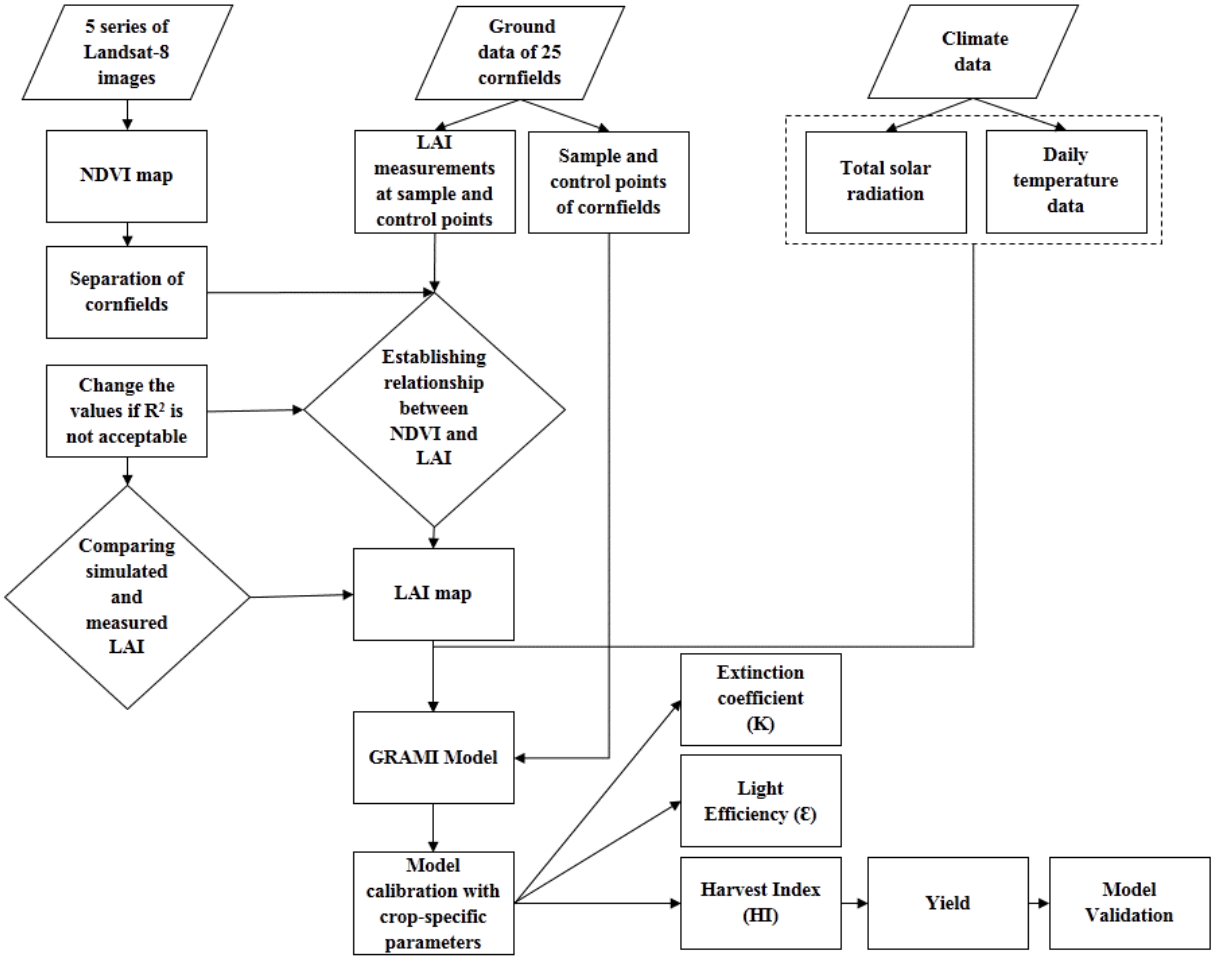

Figure 3 Schematic representation of crop yield estimation using the GRAMI model

2.3.1 Calculation of LAI and NDVI

NDVI quantifies vegetation by measuring the difference between near-infrared with wavelength about 1100–2500 nm (NIR, which vegetation strongly reflects) and red light with wavelength about 650 nm (Red, which vegetation absorbs) as shown in Equation 1. NDVI values range (-1, +1), however, there is not a distinct boundary for each type of land cover.

$$NDVI = (NIR - Red)/(NIR + Red) \quad (1)$$

LAI indicates the total ground area of leaves related to the amount of light that can be intercepted by plants. LAI can be directly calculated or indirectly estimated. In this research, LAI was calculated by green leaf area per ground surface area (Equation 2), by using the AccuPAR LP-80 Ceptometer data that was equipped with photosynthetically active radiation (PAR) sensor.

$$LAI = leaf\ area\ (m^2)\ /\ ground\ area\ (m^2) \quad (2)$$

2.3.2 GRAMI model

Inspired by the GRAMI model and remotely sensed data, corn yield was estimated. According to (Maas, 1993c), there are four steps attributed to daily corn crop growth simulation including (i) quantifying the of growing degree-days (GDD), (ii) absorption of photosynthetically active radiation by leaf, (iii) dry mass produced by the leaf canopy, and (iv) specifying LAI classification of dry mass to leaf, stem, and grain.

Equation 3 determines the increment of aggregated growing degree-days (ΔD).

$$\Delta D = Max(T - T_b, 0) \quad (3)$$

where T and T_b are the average daily air and crop-

specific base temperatures (°C), respectively. The value of T_b for corn is 10°C. When $T \leqslant T_b$, the value of ΔD is zero. The daily increase in above-ground dry mass (ΔM, g m^{-2}) was calculated using Equation 4.

$$\Delta M = \varepsilon Q \quad (4)$$

where ε is the effective radiation efficiency in g MJ^{-1} PAR and Q is the daily accumulated absorbed photosynthetically active radiation (MJ m^{-2}) absorbed by the crop canopy through Equation 5.

$$Q = \beta R(1 - e^{-K\,LAI}) \quad (5)$$

In Equation 5, β is the fraction of total solar irradiance and is valued 0.45 (Monteith and Unsworth, 2013), R is the incident daily total solar irradiance (MJ m^{-2}), LAI stands for the leaf area index, and K is a light extinction coefficient specified for a given crop.

The yield of the crop is a part of the total produced biomass equal to the harvest index based on Equation 6. According to the definition of harvest index, crop yield (kg ha^{-1}) is the ratio of grain weight to the biomass weight above the ground at the time of crop maturity.

$$Yield = HI \times M \quad (6)$$

HI (non-unit) is the harvest index (i.e., dry weight of plant m^{-2} /grain weight m^{-2}) and M is the biomass (kg ha^{-1}).

2.3.3 Statistical analysis

In this study, for model validation, values of simulated crop yield, biomass, LAI, and harvest index were compared with the measured values. Three statistical indices were used to determine the crop parameters and evaluate the performance of the model called *p*-value and R^2 using regression analysis and standard deviation. All processes of the regression model were implemented in the Statistical Package for Social Science (SPSS) software (Version 23.0). Linear regression was applied to obtain the NDVI-LAI relationship for model calibration and validation of this equation. Similarly, this procedure was applied between the weight of dry biomass (M) and the values of Q (total absorbed radiant energy) to obtain light efficiency (Ɛ) and calibration of this parameter. Moreover, linear regression was performed between the dry weight of the seeds and the total biomass at harvest time to obtain the harvest index. A level of *p*-value<0.05 was considered to statistically assess the significance of the regressions.

3 Results

3.1 NDVI and LAI maps

3.1.1 NDVI maps

In the present study, once NDVI maps have been prepared from Landsat 8 satellite imagery, the LAI values were compared with the values of the NDVI derived from the satellite image (the pixel values where the sample points were located) and the empirical relationship between these two indicators was obtained. The relationship created after validation was employed to obtain the LAI map of satellite images. The generated map was used as one of the inputs of the GRAMI model to prepare a map for crop yield. Figure 4 shows NDVI variations during corn sowing indicating that with the growth of the corn plant, the amount of NDVI increases until the corn reaches its maximum growth. After that, the amount of NDVI decreases as the corn leaves dries.

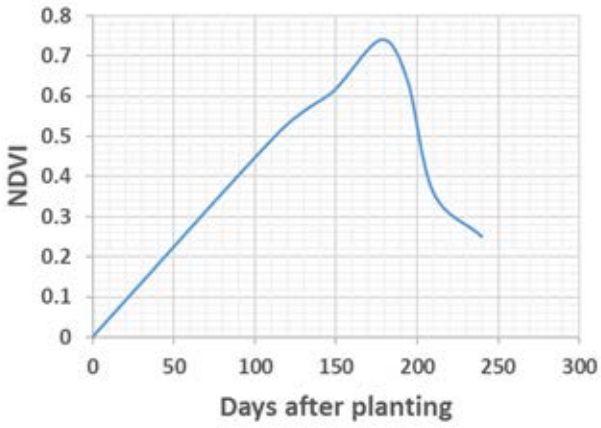

Figure 4 NDVI variations during corn sowing

3.1.2 Leaf Area Index (LAI)

The LAI value was measured at the sampling points by the ceptometer to estimate canopy PAR interception. These values were transferred to the map according to the coordinates of the harvested points. The values obtained for LAI were compared with pixel values of the NDVI map for empirical relationships. Figure 5 shows the

number of sample points and Table 1 indicates the measured LAI values, which are obtained at the time of visiting the region. In order to check data variability, Standard Deviation of LAI values was calculated with the result of 1.91, meaning that the data points tend to be very close to the mean. More precisely, the average distance between the values of the data in the set and the mean indicates an acceptable measure.

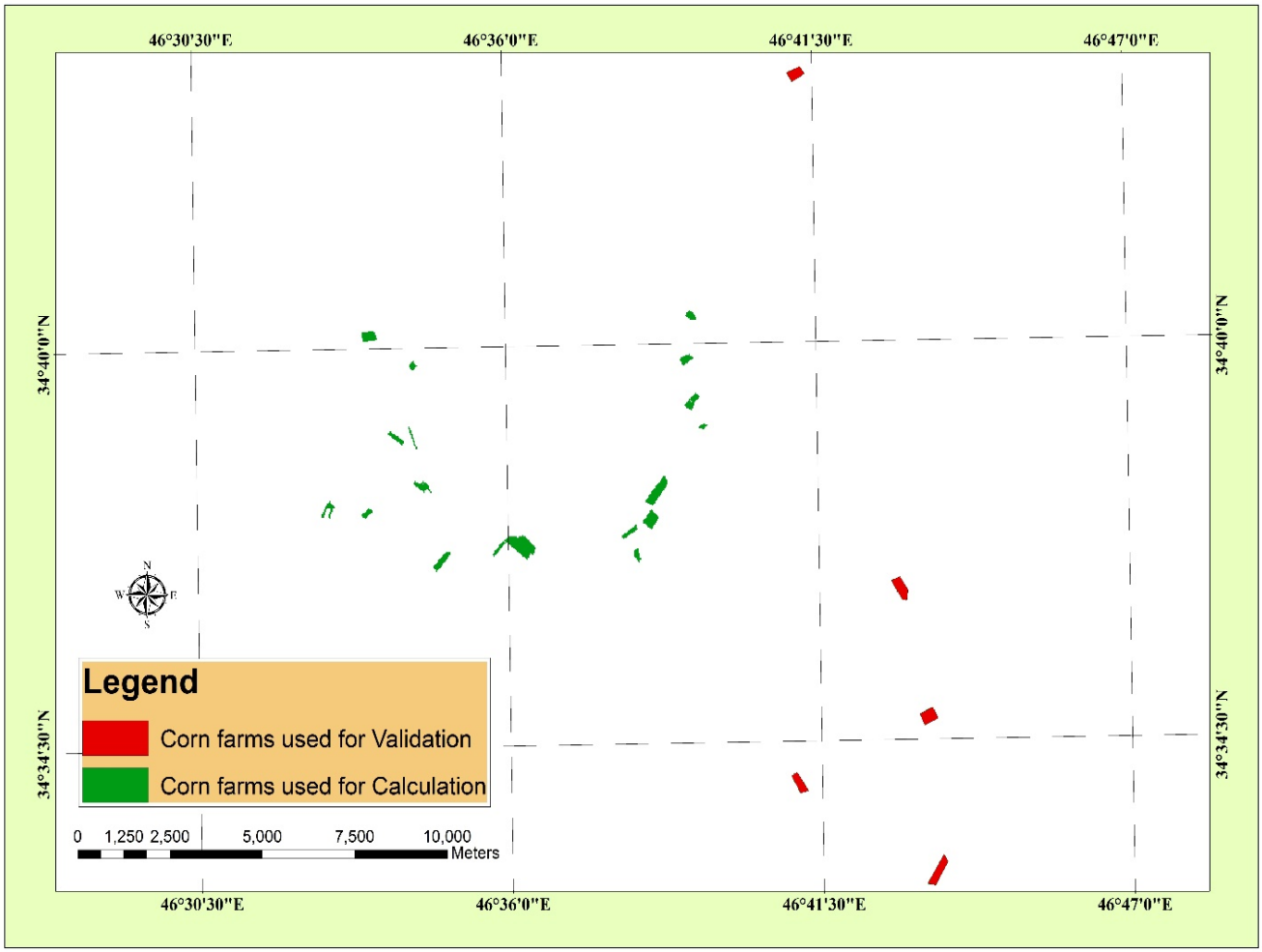

Figure 5 Selected cornfields

Table 1 Average ground LAI measured at sampling points

	May	June	July	August	September
LAI	0.94	3.64	5.49	4.69	1.81

In order to check data variability, the standard deviation of LAI values was calculated as 1.91 indicating that the data points tend to be very close to the mean.

3.1.3 Relationship between NDVI and LAI

The combination of NDVI-LAI can reveal the state of crop vegetation cover. Given the dependency of NDVI and LAI, they are able to estimate and predict crop yield (Curran, 1994). Therefore, for GRAMI model calibration, it was needed to compare the measured and simulated LAI values via obtaining a relation between LAI and NDVI that leads to obtaining the values of simulated LAI. A regression was taken between the ground LAI value and the NDVI of satellite images at 200 sample points. The highest coefficient of correlation with the coefficients of determination were 0.8 (Polynomial regression) and 0.7 (Linear regression), respectively (Figures 6 and 7. In addition, the *p*-value<0.001 indicates that using a relation between these indices has been useful to obtain simulated LAI values.

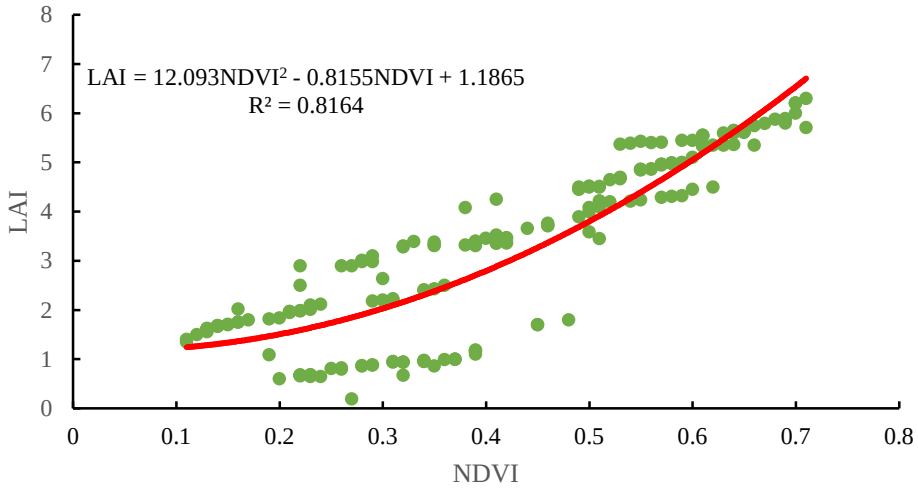

Figure 6 NDVI-LAI relationship (Polynomial regression)

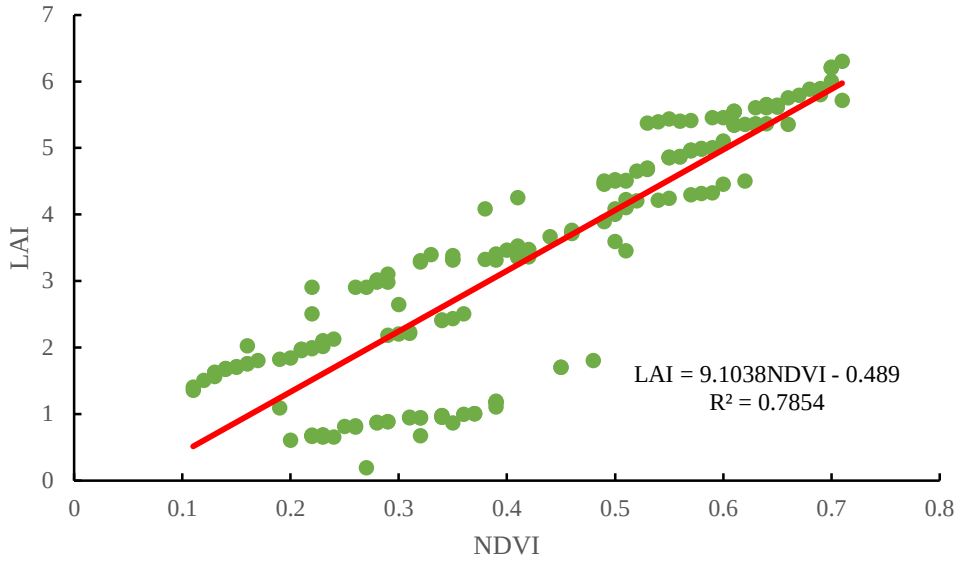

Figure 7 NDVI-LAI relationship (Linear regression)

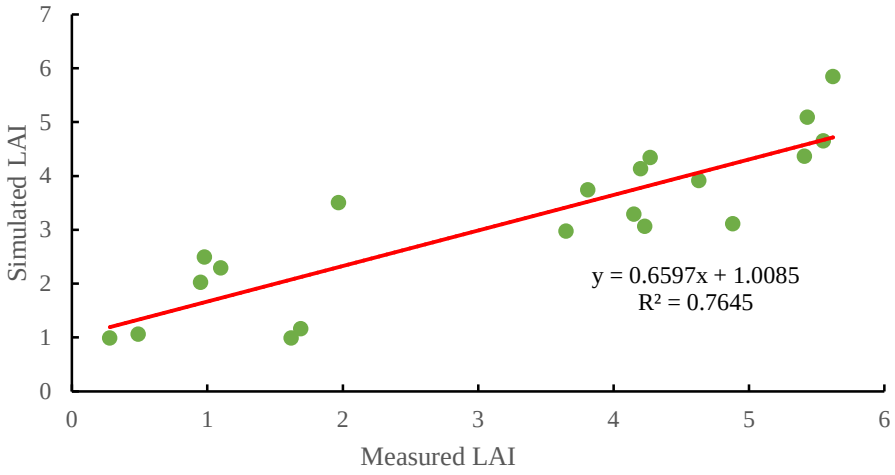

Figure 8 Relationship between measured LAI and simulated LAI at control points (Linear)

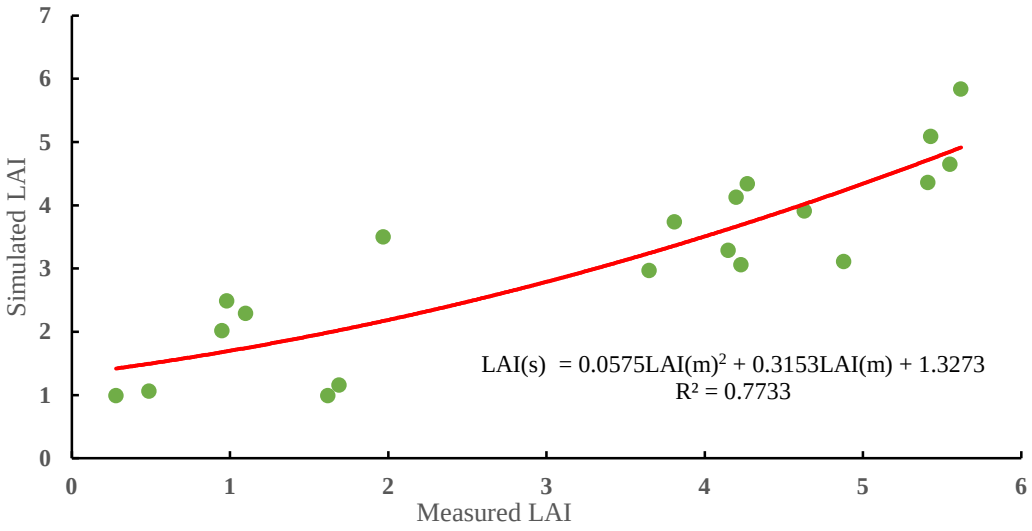

Figure 9 Relationship between measured LAI and simulated LAI at control points (Polynomial)

To validate the NDVI-LAI relationship, the LAI values, which were calculated at the control points, were compared with the LAI values of 20 ground points. The linear and polynomial regressions had R^2=0.76 and R^2=0.77, respectively (Figures 8 and 9).

3.1.4 LAI map

Five LAI maps were prepared for five periods of imagery during the corn growth to be used in the crop yield model. The map belonging to May 2016 can be seen in Figure 10 which is related to the planting stage until emergence of corn that indicates rising trend of LAI values from 1.21 to 6.87. This is the highest value at this month due to the beginning stage of flowering corn.

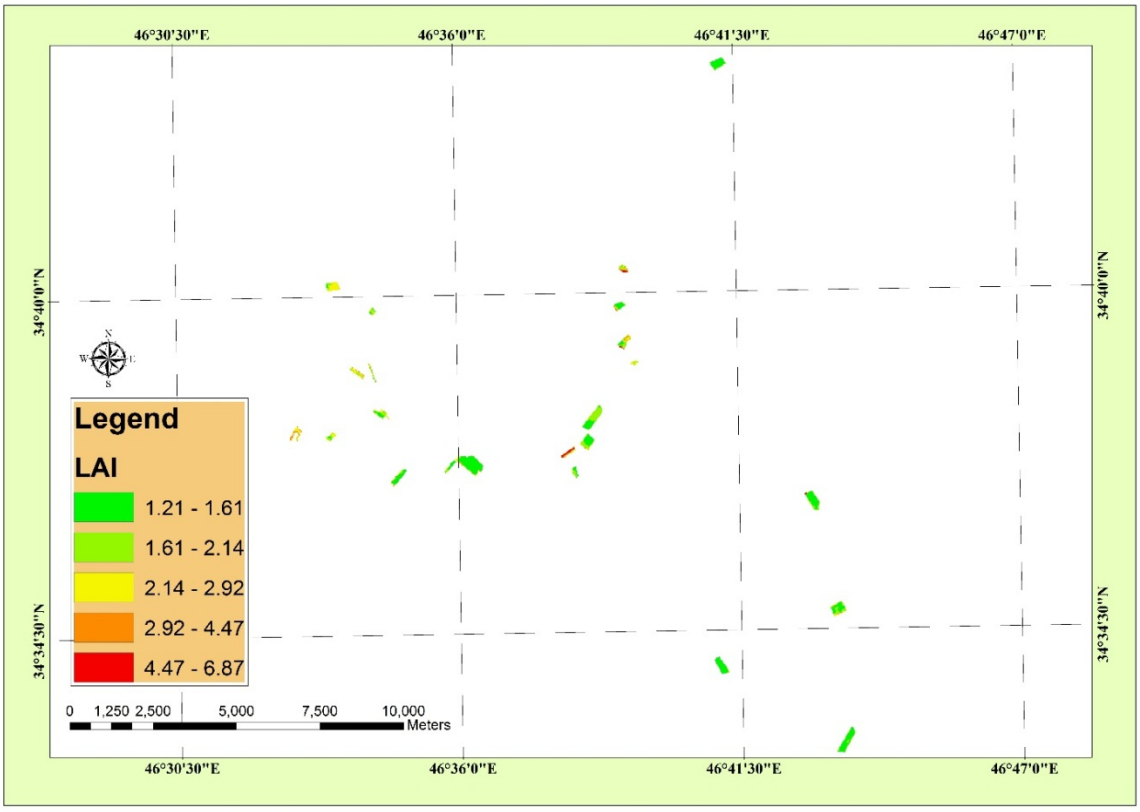

Figure 10 LAI map

3.1.5 Total solar radiation (R)

Since the meteorological stations do not harvest data from total radiation ($MJ\ m^{-2}$), the average of monthly solar radiations from Ravansar were collected. The total amount of daily radiation produced in the corn growth seasons ($W\ h\ m^{-2}$) was multiplied by 3.6 to be used in the model and converted to the unit ($MJ\ m^{-2}$) (Table 2).

Table 2 Average monthly radiation

	May	June	July	August	September
R ($W\ h\ m^{-2}$)	5.88	6.81	7.27	7.68	6.75
R ($MJ\ m^{-2}$)	21.16	24.51	26.17	27.64	24.3

3.2 Model calibration

The crop-specific parameters were calculated for the GRAMI model as follows.

3.2.1 Extinction coefficient (K)

The K value was calculated using AccuPAR by measuring the higher and lower values of PAR for corn crops when visiting the farms. The calculated value of K for each image is shown in Table 3. There is an increasing trend for K values from spring to summer.

Table 3 Calculated K value of images

	May	June	July	August	September
K	0.06	0.12	0.64	0.72	0.8

3.2.2 Light efficiency (Ɛ)

Ɛ ($g\ MJ^{-1}$) was initially valued as the slope of the regression line between the dry biomass measured in the harvest season (gm^{-2}) (M) and the total absorbed radiant energy (Q) for the sampled points. Figure 11 shows the behaviour of Q against the days that have elapsed after planting (DAP) to calculate the total PAR.

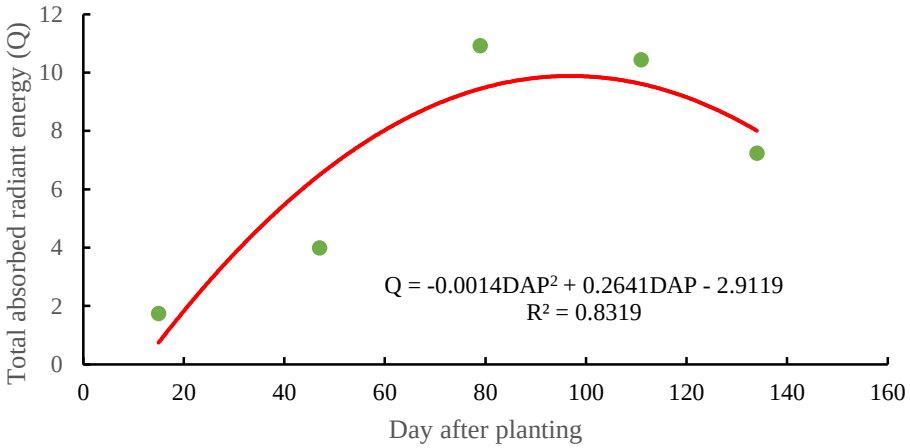

Figure 11 Total absorbed radiant energy (Q) versus the number of days after planting (DAP)

The information of 15 samples was used to determine Ɛ. The Q values were calculated for the above points.

Table 4 Regression statistic results between Q and M

Regression Statistics	
Multiple R	0.99
R Square	0.98
Adjusted R Square	0.91
Standard Error	1758.21
***p*-value**	<0.001
Observation	15
Sum of Squares	3175682883
DF	15
F	982.45

The linear regression was obtained between the weight of dry biomass (M) and the values of Q, which was Ɛ. The R^2 value was 0.98 and *p*-value<0.001 for 15 observations determine the level of trust in the predictions of the model using Q as the independent variable and M as the dependent one (Table 4).

Table 5 Slope of the linear regression between Q and M

	Coefficients	Standard Error
Intercept	0	
Q (M J m^{-2})	16.212	0.517

The coefficients and the result of the effect of each independent variable on the dependent variables were calculated. Higher the coefficient results in higher the predictive power. The best number for the calibrated light

efficiency is 16.21 MJ m^{-2} in the above regression (Table 5).

3.2.3 Harvest index (HI)

In the physiological maturity stage, samples were prepared from each plot and the harvest index was obtained by establishing the linear regression between the dry weight of the seeds and the total biomass at harvest time for the sampled points. R^2= 0.93 was calculated between dry seed weight and total dry weight, and p<0.001 indicates that regression analysis can be utilised as reliable results for obtaining harvest index.

Table 6 Error rate of corn production using GRAMI model

	May	June	July	August	September
Yield measured (kg ha^{-1})	8962.1	7853.4	8489.2	7650.47	8759.5
Simulated yield (kg ha^{-1})	7203.5	6249.6	6686.0	6448.1	7087.9
Error rate (%)	19.6	20.4	21.2	15.7	19.0

The images were included in the model in five periods to prepare the pixel map. Corn fields' maps of Ravansar city prepared and used with five LAI images related to the five stages of corn crop growth. Then, the optimization parameters obtained for Ravansar corn obtained in this study were entered into the model. Finally, by applying the harvest index, the pixel map of the whole city was obtained. The map of corn yield in Figure 12 demonstrates five categories of corn yield estimation of the city classified from 2334.39 to 8375.18 kg ha^{-1}, which is the prediction of yield estimated belonging to the year 2016 for the region.

3.3 Model validation

The mean crop of each of the five farms used in the validation was considered to be the simulated crop for evaluating the production error rate. The error rate of the GRAMI model in the estimation of the corn yield was calculated by comparing the land measurement data of the studied fields and values simulated by the model. Table 6 shows the error rates of using the model in the experimental fields. According to the results obtained in this study, the model is valid with a mean error of 19.21%.

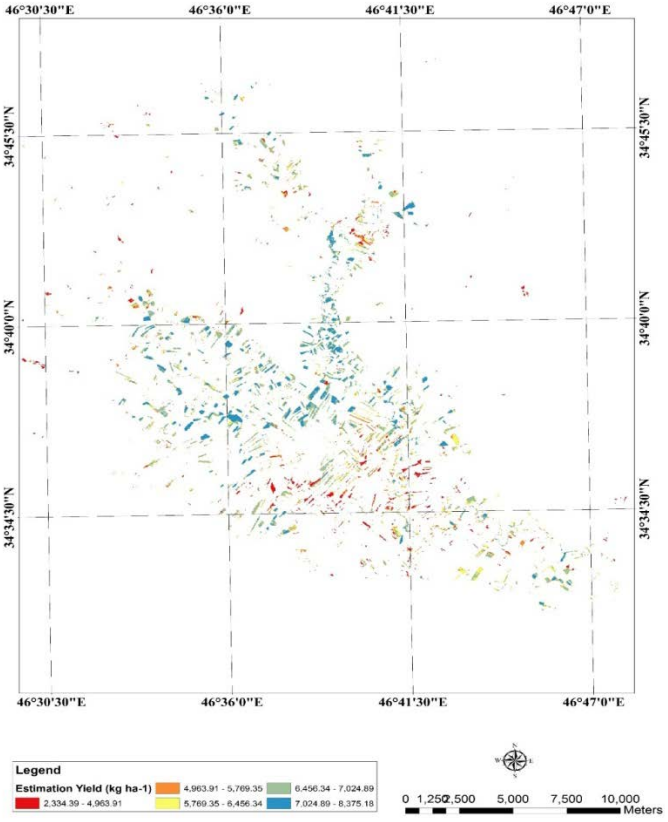

Figure 12 Corn yield prediction map in Ravansar

4 Discussion

The feasibility of the GRAMI-corn model for crop growth and grain yield estimation using Landsat 8 satellite images and atmospheric data was evaluated for a semi-arid area. Although twenty-five corn farms were selected to assess the practicality of the model, the predicted map of corn yield estimation of the whole city was obtained.

This research applied GRAMI model and climate data to estimate corn yield. Compared to other models and dataset that used the GRAMI model for crop monitoring, the finding of this research for corn estimation is acceptable. Using the SAFY-WB agrometeorological model along with optical and synthetic aperture radar satellite images and weather data (solar radiation, rainfall, air temperature, wind speed, and relative humidity) resulted in relative errors inferior to 13.95% (R^2 > 0.69) (Yeom et al., 2018). Another study employed the piecewise linear regression method with breakpoint and considered NDVI, soil moisture, surface temperature, and rainfall data for yield prediction of corn and soybean with promising results of R^2 = 0.78 and R^2 = 0.86, respectively (Prasad et al., 2006). Therefore, the absolute error and accuracy between the average estimated and the average observed yield values reported for this study (19.21% and 80.79%, respectively) certifies that integrating climatic data with the GRAMI model for corn estimation is effective.

Several studies have applied GRAMI model to estimate other crop yields such as wheat, cotton, rice, and sorghum. The absolute errors for wheat were 5.44% and 6.86% for two seasons (Padilla et al., 2012), 5.8% (Maas, 1993c), and with final yield estimation of 25.9% (Atzberger and Eilers, 2011). The absolute errors for grain sorghum was 2% (Maas, 1988a, 1988b). Additionally, applying GRAMI model for rice demonstrated significant range of accuracy. Examples of these implementations are the standard errors of 0.45, 0.27, and 0.52 between simulated and measured mean values obtained from paired *t*-tests (α = 0.05) by using coverage of unmanned aerial vehicle (UAV) and RapidEye satellite images (Kim et al., 2017) and standard errors of 0.183, 0.075, and 0.101 between simulated and observed paddy yields obtained from *t*-testing procedure using Geostationary Ocean Color Imager (GOCI) and MODIS combined with meteorological parameters such as solar insolation and air temperature (Yeom et al., 2018). These result justify the performance of GRAMI rice model for paddy rice's growth estimation (Yeom et al., 2015). Therefore, the *p*-value (<0.05), R^2 (0.81, 0.77, 0.98, and 0.93), and standard deviation (1.91) obtained in the relevant steps were rational and trustworthy in this research.

A number of factors can contribute to the magnitude of estimation errors for corn fields that can stem from the characteristics of the corn in using different models and parameters, using only one type of satellite imagery, one year for assessment, limited ground and satellite parameters, not using multiple VIs, or human and machine errors. For example, yield values reported by farmers can result in estimation errors in this study. However, estimation of corn using GRAMI model incorporated with meteorological data has not been applied for higher evaluation and calibration. The results showed that the GRAMI-corn model successfully estimated grain yield of corn by map projections over the studied period. The GRAMI model with the ability to perform within-season calibration reproduces crop growth and grain yields using remotely sensed data. Thereby, it is functional for monitoring crop growth conditions and determining grain yield. Minimizing the error between simulated and observed canopy growth variables was justified by combining the GRAMI-corn model and LAI value (Kim et al., 2015). However, the final accuracy can be increased if high-resolution satellites images are coupled with other remote sensing data and ground measurements.

5 Conclusion

A GRAMI model was developed for temporally monitoring corn yields at regional scale. In this context, the use of climate data combined with satellite imagery

and ground data constitutes a useful tool for accurate monitoring of corn yields. Results of temporal monitoring corn yields over five months in a semiarid region in Western Iran (the city Ravansar) using this model demonstrated reasonable consistency between observed and estimated yields. In terms of model accuracy, the average amount that a field is under- or over-estimated as corn yield is approximately 19% of the average five months yield observation for the region. It was shown that, the spatial and temporal features for corn yield estimation is sensitive to meteorological factors, as it has been proved in literature for other agricultural products too. In conclusion, the GRAMI-corn model enriched by climate data and calibrated using satellite imagery become a useful tool to be exerted to wide agroclimatic areas and to be extended to additional crops. For future studies, the GRAMI model performance can be examined and incorporated with other acceptable models especially for corn yield estimation in tropical and sub-tropical regions and areas with different environmental and climatic conditions, various soil and other required factors related to crop growth with agroclimatic constraints. More accurate local climatic measurements (temperature, radiation, etc.), collected from networked weather stations, can calibrate the model to consider for a good estimate of crop yields.

References

Alharbi, S., W. R. Raun, D. B. Arnall, and H. Zhang. 2019. Prediction of maize (*Zea mays* L.) population using normalized-difference vegetative index (NDVI) and coefficient of variation (CV). *Journal of Plant Nutrition*, 42(6): 673-679.

Ameline, M., R. Fieuzal, J. Betbeder, J. F. Berthoumieu, and F. Baup. 2018. Estimation of corn yield by assimilating SAR and optical time series into a simplified agro-meteorological Model: from diagnostic to forecast. *IEEE Journal of Selected Topics in Applied Earth Observations and Remote Sensing*, 11(12): 4747-4760.

Atzberger, C., and P. H. C. Eilers. 2011. Evaluating the effectiveness of smoothing algorithms in the absence of ground reference measurements. *International Journal of Remote Sensing*, 32(13): 3689-3709.

Basso, B., and L. Liu. 2019. Seasonal crop yield forecast: Methods, applications, and accuracies. *In Advances in Agronomy*, vol. 154, ed. D. L. Sparks, ch. 4, 201-255. United States: Academic Press.

Butler, E. E., and P. Huybers. 2013. Adaptation of US maize to temperature variations. *Nature Climate Change*, 3(1): 68-72.

Climate-Data. 2016. Climate data for cities worldwide. Available: https://en.climate-data.org/. Accessed 1 November 2016.

Curran, P. J. 1994. Imaging spectrometry. *Progress in Physical Geography*, 18(2): 247-266.

Dahikar, S. S., and S. V. Rode. 2014. Agricultural crop yield prediction using artificial neural network approach. *International Journal of Innovative Research in Electrical, Electronics, Instrumentation and Control Engineering*, 2(1): 683-686.

Di Paola, A., R. Valentini, and M. Santini. 2016. An overview of available crop growth and yield models for studies and assessments in agriculture. *Journal of the Science of Food and Agriculture*, 96(3): 709-714.

Doraiswamy, P. C., S. Moulin, P. W. Cook, and A. Stern. 2003. Crop yield assessment from remote sensing. *Photogrammetric Engineering & Remote Sensing*, 69(6): 665-674.

Drusch, M., U. Del Bello, S. Carlier, O. Colin, V. Fernandez, F. Gascon, B. Hoersch, C. Isola, P. Laberinti, P. Martimort, A. Meygret, F. Spoto, O. Sy, F. Marchese, and P. Bargellini. 2012. Sentinel-2: ESA's optical high-resolution mission for gmes operational services. *Remote Sensing of Environment*, 120: 25-36.

FAOSTAT. 2016. Food and agriculture data. Available: http://www.fao.org/faostat/en/#data/QC/visualize. Accessed 23 May 2018.

Hoefsloot, P., A. V. Ines, J. C. V. Dam, G. Duveiller, F. Kayitakire, and J. Hansen. 2012. Combining crop models and remote sensing for yield prediction: Concepts, applications and challenges for heterogeneous smallholder environments. Report of CCFAS-JRC Workshop at Joint Research Centre. Luxembourg: Publications Office of the European Union.

Jeong, S., J. Ko, J. Choi, W. Xue, and J. M. Yeom. 2018a. Application of an unmanned aerial system for monitoring paddy productivity using the GRAMI-rice model. *International Journal of Remote Sensing*, 39(8): 2441-2462.

Jeong, S., J. Ko, M. Kang, J. Yeom, C. T. Ng, S. H. Lee, Y. G. Lee, and H. Y. Kim. 2020. Geographical variations in gross primary production and evapotranspiration of paddy rice in the Korean Peninsula. *Science of The Total Environment*, 714:

136632.

Jeong, S., J. Ko, and J. M. Yeom. 2018b. Nationwide projection of rice yield using a crop model integrated with geostationary satellite imagery: A case study in South Korea. *Remote Sensing*, 10(10): 1665.

Kamir, E., F. Waldner, and Z. Hochman. 2020. Estimating wheat yields in Australia using climate records, satellite image time series and machine learning methods. *ISPRS Journal of Photogrammetry and Remote Sensing*, 160: 124-135.

Khaki, S., L. Wang, and S. V. Archontoulis. 2020. A cnn-rnn framework for crop yield prediction. *Frontiers in Plant Science*, 10: 1750.

Kim, H., J. Ko, S. Jeong, J. Yeom, J. O. Ban, and H. Y. Kim. 2015. Simulation and mapping of rice growth and yield based on remote sensing. *Journal of Applied Remote Sensing*, 9(1): 096067.

Kim, M., J. Ko, S. Jeong, J. M. Yeom, and H. O. Kim. 2017. Monitoring canopy growth and grain yield of paddy rice in South Korea by using the GRAMI model and high spatial resolution imagery. *GIScience & Remote Sensing*, 54(4): 534-551.

Ko, J., S. J. Maas, R. J. Lascano, and D. Wanjura. 2005. Modification of the GRAMI model for cotton. *Agronomy Journal*, 97(5): 1374-1379.

Maas, S. J. 1988a. Using satellite data to improve model estimates of crop yield. *Agronomy Journal*, 80(4): 655-662.

Maas, S. J. 1988b. Use of remotely-sensed information in agricultural crop growth models. *Ecological Modelling*, 41(3-4): 247-268.

Maas, S. J. 1992. GRAMI: A crop growth model that can use remotely sensed information. Weslaco, TX: ARS-US Department of Agriculture, Agricultural Research Service (USA).

Maas, S. J. 1993a. Parameterized model of gramineous crop growth: I. Leaf Area and dry mass simulation. *Agronomy Journal*, 85(2): 348-353.

Maas, S. J. 1993b. Parameterized model of gramineous crop growth: II. Within-season simulation calibration. *Agronomy Journal*, 85(2): 354-358.

Maas, S. J. 1993c. Within-season calibration of modeled wheat growth using remote sensing and field sampling. *Agronomy Journal*, 85(3): 669-672.

Monteith, J., and M. Unsworth. 2013. *Principles of Environmental Physics: Plants, Animals, and the Atmosphere*. 4th ed. Burlington, MA: Academic Press.

Moran, M. S., S. J. Maas, and P. J. Pinter Jr. 1995. Combining remote sensing and modeling for estimating surface evaporation and biomass production. *Remote Sensing Reviews*, 12(3-4): 335-353.

Moulin, S., A. Bondeau, and R. Delecolle. 1998. Combining agricultural crop models and satellite observations: From field to regional scales. *International Journal of Remote Sensing*, 19(6): 1021-1036.

Nguyen, V. C., S. Jeong, J. Ko, C. T. Ng, and J. Yeom. 2019. Mathematical integration of remotely-sensed information into a crop modelling process for mapping crop productivity. *Remote Sensing*, 11(18): 2131.

Oteng-Darko, P., S. Yeboah, S. N. T. Addy, S. Amponsah, and E. O. Danquah. 2013. Crop modeling: A tool for agricultural research–A review. *Journal of Agricultural Research Development*, 2(1): 1-6.

Padilla, F. L. M., S. J. Maas, M. P. González-Dugo, F. Mansilla, N. Rajan, P. Gavilán, and J. Domínguez. 2012. Monitoring regional wheat yield in Southern Spain using the GRAMI model and satellite imagery. *Field Crops Research*, 130: 145-154.

Prasad, A. K., L. Chai, R. P. Singh, and M. Kafatos. 2006. Crop yield estimation model for Iowa using remote sensing and surface parameters. *International Journal of Applied Earth Observation and Geoinformation*, 8(1): 26-33.

Rauff, K. O., and R. Bello. 2015. A review of crop growth simulation models as tools for agricultural meteorology. *Agricultural Sciences*, 6(9): 1098-1105.

Roy, D. P., M. A. Wulder, T. R. Loveland, C. E. Woodcock, R. G. Allen, M. C. Anderson, D. Helder, J. R. Irons, D. M. Johnson, R. Kennedy, T. A. Scambos, C. B. Schaaf, J. R. Schott, Y. Sheng, E. F. Vermote, A. S. Belward, R. Bindschadler, W. B. Cohen, F. Gao, J. D. Hipple, P. Hostert, J. Huntington, C. O. Justice, A. Kilic, V. Kovalskyy, Z. P. Lee, L. Lymburner, J. G. Masek, J. McCorkel, Y. Shuai, R. Trezza, J. Vogelmann, R. H. Wynne, and Z. Zhu. 2014. Landsat-8: Science and product vision for terrestrial global change research. *Remote Sensing of Environment*, 145: 154-172.

Sharif, M., and A. A. Alesheikh. 2018. Context-aware movement analytics: implications, taxonomy, and design framework. *WIREs Data Mining and Knowledge Discovery*, 8(1): e1233.

Shawon, A. R., J. Ko, B. Ha, S. Jeong, D. K. Kim, and H.-Y. Kim. 2020. Assessment of a proximal sensing-integrated crop model for simulation of soybean growth and yield. *Remote Sensing*, 12(3): 410.

Tashayo, B., A. Honarbakhsh, M. Akbari, and M. Eftekhari. 2020. Land suitability assessment for maize farming using a GIS-AHP method for a semi- arid region, Iran. *Journal of the Saudi Society of Agricultural Sciences*, 19(5): 332-338.

Torres, R., P. Snoeij, D. Geudtner, D. Bibby, M. Davidson, E. Attema, P. Potin, B. Rommen, N. Floury, M. Brown, I. N. Traver, P. Deghaye, B. Duesmann, B. Rosich, N. Miranda, C. Bruno, M. L'abbate, R. Croci, A. Pietropaolo, M. Huchler, and F. Rostan. 2012. GMES Sentinel-1 mission. *Remote Sensing of Environment*, 120: 9-24.

USGS. 2016. United States Geological Survey. Available: https://www.usgs.gov/. Accessed 1 November 2016.

Van Ittersum, M. K., K. G. Cassman, P. Grassini, J. Wolf, P. Tittonell, and Z. Hochman. 2013. Yield gap analysis with local to global relevance—a review. *Field Crops Research*, 143: 4-17.

Van Wart, J., K. C. Kersebaum, S. Peng, M. Milner, and K. G. Cassman. 2013. Estimating crop yield potential at regional to national scales. *Field Crops Research*, 143: 34-43.

Xu, X., P. Gao, X. Zhu, W. Guo, J. Ding, C. Li, M. Zhu, and X. Wu. 2019. Design of an integrated climatic assessment indicator (ICAI) for wheat production: A case study in Jiangsu Province, China. *Ecological Indicators*, 101: 943-953.

Yeom, J.-M., S. Jeong, G. Jeong, C. T. Ng, R. C. Deo, and J. Ko. 2018. Monitoring paddy productivity in North Korea employing geostationary satellite images integrated with GRAMI-rice model. *Scientific Reports*, 8(1): 1-15.

Yeom, J.-M., J. Ko, and H.-O. Kim. 2015. Application of GOCI-derived vegetation index profiles to estimation of paddy rice yield using the GRAMI rice model. *Computers and Electronics in Agriculture*, 118: 1-8.

Zipper, S. C., J. Qiu, and C. J. Kucharik. 2016. Drought effects on US maize and soybean production: spatiotemporal patterns and historical changes. *Environmental Research Letters*, 11(9): 094021.